

## Comparative analysis of turbulence models in hydraulic jumps

Raquel J. Lobosco<sup>\*1</sup>, David O. da Fonseca<sup>1</sup>, Graziella M. F. Jannuzia<sup>2a</sup>  
and Necesio G. Costa<sup>1</sup>

<sup>1</sup>Thermal and Fluids Laboratory, Rio de Janeiro Federal University, Macaé Campus, Brazil

<sup>2</sup>Field Testing and Instrumentation Laboratory Prof Márcio Miranda Soares,  
COPPE and Rio de Janeiro Federal University, Macaé Campus, Brazil

(Received October 1, 2018, Revised May 3, 2019, Accepted June 20, 2019)

**Abstract.** A numerical simulation of the incompressible multiphase hydraulic jump flow was performed to compare the interface prediction through the use of the three RANS turbulence models:  $k-\epsilon$ , RNG  $k-\epsilon$  and SST  $k-\omega$ . A three dimensional no submerged hydraulic jump and a two dimensional submerged hydraulic jump were modeled. Both the geometry and the mesh were created using the open source Gmsh code. The project's geometry consists of a rectangular channel with length and height differences between the two dimensional and three dimensional simulations. Uniform hexahedral cells were used for the mesh. Three refining meshes were constructed to allow to verify simulation convergence. The Volume of Fluid (abbr. VOF) method was used for treatment of the air-water surface. The turbulence models were evaluated in three distinct set up configurations to provide a greater accuracy in the flow representation. In the two-dimensional analysis of a submerged hydraulic jump simulation, the turbulence model RNG  $k-\epsilon$  provided a better interface adjust with the experimental results than the model  $k-\epsilon$  and SST  $k-\omega$ . In the three-dimensional simulation of a no-submerged hydraulic jump the  $k-\epsilon$  showed better results than the SST  $k-\omega$  and RNG  $k-\epsilon$  capturing the height and length of the ledge with a better fit with the experimental results.

**Keywords:** fluid-flow interface; turbulence model; hydraulic jump; multiphase flow

### 1. Introduction

Hydraulic jumps occur due to the rapid transition from supercritical to subcritical flow, associated with a sudden elevation of water level, surface waves and air bubble entrainment. Analytical solutions of the hydraulic jump were presented by McCarthy O'Leary (1978), who implemented an analysis of the study of the propagation of the jump in a channel of uniform width and variable length. In particular, they derived a differential equation and determined how the height varies with the wave propagation. Thus, they established criteria for the wave to grow, decay or to propagate with constant amplitude. Three years later, Hirt and Nichol (1981) introduced the famous Volume of Fluid method. This method has been shown to be more flexible

---

\*Corresponding author, Professor, E-mail: [rlobosco@macae.ufrj.br](mailto:rlobosco@macae.ufrj.br)

and efficient than old methods for dealing numerically with prediction of complex free surface.

This paper is essentially concerned by the numerical investigation of the fluid-flow interface interactions that may appear between the air bubbles and the droplets of water in the deformable interface in the channel that lead to the hydraulic jump. Numerical simulation of interface flow prediction has improved in the last decades through the new numerical methods Volume of Fluid and Level-set. It allows to represent the experimental results in an accurate way coupling the multiphase flow phases in the mesh interface cells.

## 2. Mathematical models for multiphase interface flow

The fluid volume method was used assuming two immiscible fluids, air and water. A scalar alpha parameter is used to define the volume of fluid 1, denoted by  $V_1$ , in each element. In this way,  $V_2$  (the volume of the second fluid) is simply  $1 - \alpha$  and the volume fraction of the cell occupied by a certain fluid is given by  $\alpha = V_1/V$ . The unit value corresponds to the filled cell of a given fluid while the null value indicates that the cell does not contain this fluid. Cells with values between zero and one represent the interface. The monitoring of the air-water interface is given by the solution of the Continuity Equation, Eq. (1).

$$\frac{\partial \alpha}{\partial t} + \Delta \cdot (\alpha \vec{u}) = 0 \quad (1)$$

For an incompressible Newtonian fluid flow, Eq. (2) represents the momentum conservation, known as the Navier-Stokes Equation.

$$\rho \frac{\partial}{\partial t} v = -\nabla p + \mu \nabla^2 v + \rho g \quad (2)$$

The decomposition of the flow properties is given through the Eq. (3), which allows to write the variables in terms of their temporal means, when applied in the Navier-Stokes equations, we obtain the mean Reynolds equations (RANS). Thus, each quantity of the flow will have its random variable (float) around the mean value in time, (Piomelli 1999).

$$\bar{f} = \frac{1}{\Delta t} \int_t^{\Delta t} f(\tau) dt \quad (3)$$

Being  $f$  a flow property and  $\bar{f}$  its mean. As a result, in the average Reynolds equations, a new turbulence-related term  $(-\rho \bar{u}'_i \bar{u}'_j)$ , appears, since  $\bar{u}'_i$  is related to speed fluctuation. This term is  $i j$  is called Reynolds tensor

$$\tau_{ij} = -\rho \bar{u}'_i \bar{u}'_j \quad (4)$$

Thus, the mean Reynolds equations and the continuity equation do not form a closed system, since there are more unknowns variables than equations. The fluctuations that appear in the Reynolds tensor need to be modeled to close the system, the so called closing models are then used.

### 2.1 Closure turbulence model $k - \epsilon$

The closure model  $k - \epsilon$  is based on the concept of turbulent viscosity. In this model, the characteristic turbulence scales are represented by two turbulent variables, called the turbulent

kinetic energy  $k$  and energy dissipation rate  $\epsilon$ , thus creating two more equations for each variable. Thus, the turbulent viscosity is defined as  $\mu_t = C_\mu k^2 / \epsilon$ , where  $C_\mu$  is an empirical coefficient. The formulation of this model is given by Eq. (5) and (6).

$$\frac{\partial}{\partial t}(\rho k) + \frac{\partial}{\partial x_i}(\rho k u_i) = \frac{\partial}{\partial x_j} \left[ \left( \mu + \frac{\mu_t}{\sigma_k} \right) \frac{\partial k}{\partial x_j} \right] + P_k + P_b - \rho \epsilon - Y_M + S_k \quad (5)$$

$$\frac{\partial}{\partial t}(\rho \epsilon) + \frac{\partial}{\partial x_i}(\rho \epsilon u_i) = \frac{\partial}{\partial x_j} \left[ \left( \mu + \frac{\mu_t}{\sigma_\epsilon} \right) \frac{\partial \epsilon}{\partial x_j} \right] + C_{1\epsilon} \frac{\epsilon}{k} (P_k + C_{3\epsilon} P_b) - C_{2\epsilon} \rho \frac{\epsilon^2}{k} + S_\epsilon \quad (6)$$

In that  $t$  is time,  $\rho$  specific mass,  $x_i$  the coordinate in the axis  $i$ ,  $\mu$  dynamic viscosity,  $\mu_t$  turbulent viscosity,  $P_k$  is the product of turbulent kinetic energy,  $P_b$  is the effect of buoyancy  $Y_m$  dilatation effect,  $S_k$  and  $S_\epsilon$  epsilon are the average tensor models of the tension. The remaining terms ( $C_\mu$ ,  $C_{1\epsilon}$ ,  $C_{2\epsilon}$ ,  $C_{3\epsilon}$ ,  $\sigma_k$  and  $\sigma_\epsilon$ ) are transport coefficients which in this model are respectively 0.09, 1.44, 1.92, -0.33, 1.0 and 1.3, as cited by (Versteeg and Malalasekera 1995).

## 2.2 Closure turbulence model RNG $k-\epsilon$

The closing model RNG  $k-\epsilon$  was introduced in the literature by Yakhot and Smith (1992) by adopting the renormalization group theory (RNG) to modify the Navier-Stokes equations. This modification considers the effects of the small scales, which are represented by the modified transport coefficients, so their equations are very similar to the Eqs. (5) and (6). According to [5], the model RNG  $k-\epsilon$  is cited to be the most used model in hydraulic applications.

## 2.3 Closure turbulence model SST $k-\omega$

The closure model  $k-\omega$  is also based on the concept of turbulent viscosity, where the turbulent variables are the turbulent kinetic energy ( $k$ ) and the specific dissipation rate ( $\omega$ ), being  $\omega$  interpreted as a ratio of  $\epsilon$  and  $k$ . According to Bayon and Lopez (2015) several authors claim that the  $k-\epsilon$  and RNG  $k-\epsilon$  models are not suitable for cases that contain large flows of adverse pressure. To solve this problem the  $k-\omega$  model was introduced. Among the existing  $k-\omega$  models, SST  $k-\omega$  showed a better performance over the original model and  $k-\omega$ , as cited at (Bayon and Lopez 2015).

## 3. Numerical results

The purpose of this study was to compare the turbulence models in the numerical simulation problems of hydraulic jump in open channels. In order to validate which model of turbulence had the highest accuracy, a comparison with the experimental, two-dimensional results were proceed with the results described by Long *et al.* (1990). And the three-dimensional comparison is based on the experimental results described by Wang *et al.* (2015). In this way a total of fifteen simulations were developed. Three in the two-dimensional case plus two in the three-dimensional setup were investigated. Both studies were made to verify which of the inserted turbulence model has greater accuracy in representing the air-water interface in a hydraulic jump. In particular, the height of the hydraulic jump is denominated ( $h_r$ ) and the ( $L_r$ ) is the length.

The hydraulic jumps can be characterized by the Froude number. Above the unit, the Froude

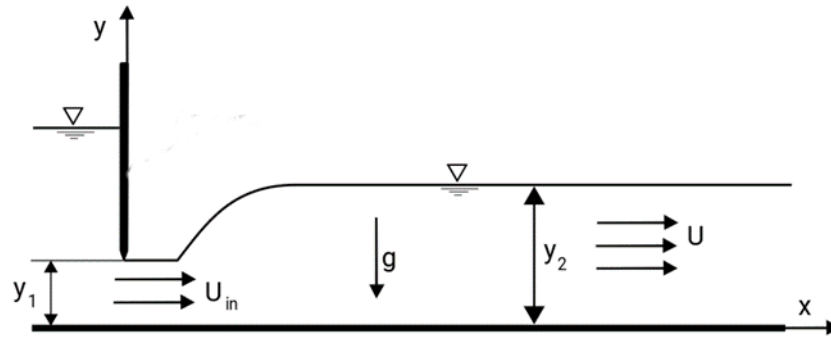


Fig. 1 Parameters of the hydraulic jump

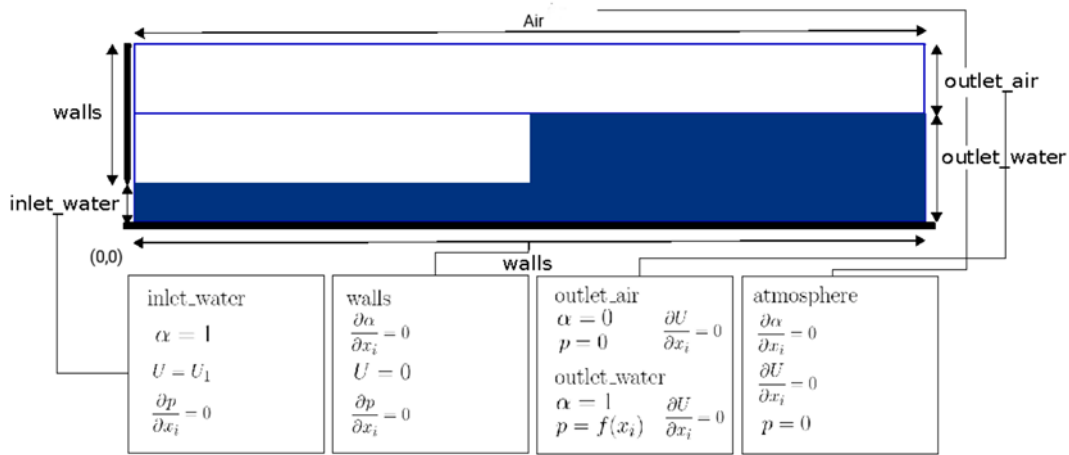


Fig. 2 Boundary conditions

number defines the flow as supercritical, below as subcritical. The adimensional Froude number is defined by Eq. (7).

$$Fr = \frac{U}{\sqrt{gy}} \tag{7}$$

in which U is the fluid velocity, g gravity acceleration and y flow depth. Fig. 1 shows the supercritical depth (y1), conjugate depth (y2), length (hr) and height (h) of the hydraulic jump that is given by the differences between the depths (y1) and (y2).

### 3.1 Boundary conditions

Six different contour conditions were defined, which are: walls, inlet\_water, outlet\_air, outlet\_water, atmosphere and empty/slip, being empty for the laterals of the two-dimensional case and slip for the three-dimensional. To elaborate these boundary conditions, three blocks were constructed in the Gmsh. Gmsh was chosen as the production of mesh geometry for its simplicity and ease of use.

Fig. 2 represents the boundary conditions used in both, the two-dimensional and the three-

dimensional case. The volumetric fraction is represented by  $\alpha$ . when  $\alpha$  is equals 1, the cell contains 100% water and when  $\alpha$  equal to 0, it is a 100% air. In this way the boundary condition of  $\alpha$  equal to 1 represent the volume of water that is entering (inlet\_water) and the volume of water that is leaving the domain (outlet\_water). In the input condition, since velocity is defined as  $U_1$  the pressure is solved in an algebraic system of equations and have its value as a function of velocity, so it is defined as a gradient equal to zero. Similarly, in the outlet condition, the pressure is defined as a function of the volume of water filled ( $p = \rho g y_2$ ) and the velocity that is solved in an algebraic system of equations.

In the OpenFoam multiphase solver, called interFoam, the hydrostatic pressure of the system is defined, so  $p = 0$  represents the atmospheric pressure, which is used both in the outlet condition and in the contour condition atmosphere. In the wall boundary condition, the velocity is set to zero according to the non-slip condition, consequently the pressure gradient is set to zero. The  $\alpha$  gradient is assigned zero as well, resulting in a fixed value for that solid wall variable. The contour condition on the sides of the system is different for the two-dimensional and three-dimensional case. Whereas in the first, the boundary condition is empty, in the second it is slip. The empty condition prevents from solving the variables in the third dimension (z-axis). The slip condition decreases the computational resource by shortening the channel width of 0.5 m to 0.2 m.

#### 4. Bidimensional analysis

Nine different cases were performed for the analysis of the submerged hydraulic jump based on the experimental results reproduced by D. Long, Steffler and Rajaratnam. (1990). Those experiments were called experiments 3, 6 and 8 with the Froude numbers of 3.19, 5.49 and 8.19, respectively. For each case, a comparative analysis of the numerical turbulence models were proceeded.

Three of the ten experiments reproduced by , Steffler and Rajaratnam. (1990) were numerically evaluated as showed in Table 1.

The stability convergence were checked, for each property, by the residual time step before any quantitative analysis. The analysis of the initial residue of each system variable and the solution stability over time were evaluated.

Table 1 Bi-dimensional simulation setup, adapted from Steffler and Rajaratnam (1990)

Experiment	$y_1$ (m)	$U_1$ (m/s)	$y_1 + y_t$ (m)	Fr	$Re(\times 10^{-3})$
3	0.025	1.58	0.187	3.19	3.95
6	0.025	2.71	0.299	5.49	6.80
8	0.015	22.55	23.63	23.12	22.73

Table 2 Relative Error - Experiment 3

Model	er (%)	
	Lr	Hr
k- $\epsilon$	9.00	31.09
SST k- $\omega$	59.60	12.81
RNG k- $\epsilon$	2.32	16.46

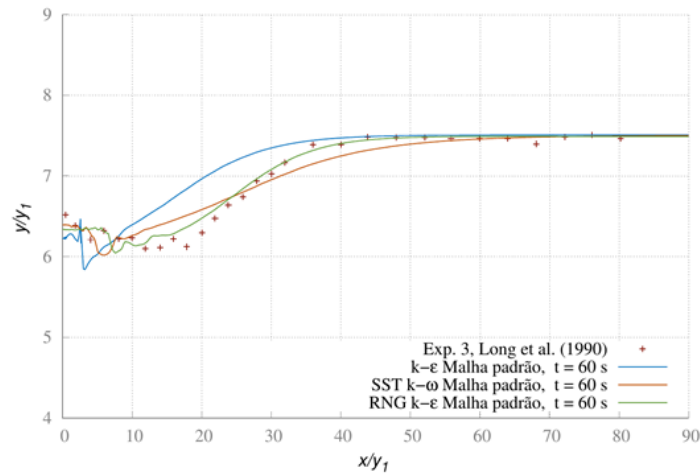


Fig. 3 Turbulence model analysis of experiment 3

#### 4.1 Experiment 3

This experiment consists of an initial velocity  $U_1 = 1.58$  m/s, depth of supercritical flow  $y_1 = 0.025$  m and Froude number of  $Fr = 3.19$ . The solution rotated to 60s with a standard mesh refinement for the three turbulence models.

In relation to the height of the hydraulic jump, which is given by the difference of the supercritical depth ( $y_1$ ) with the conjugate depth ( $y_2$ ), from the dimensionless length 60 ( $X/y_1$ ), both models obtain the same result. However, in relation to the shoulder length, which is a sensitive variable of the phenomenon, the model  $k-\epsilon$  predicts the phenomena more accurately than the SST  $k-\omega$  model. In the model SST  $k-\omega$ , the length of the hydraulic jump extends to the dimensionless length 60, whereas in the model  $k-\epsilon$  the stability is around the value 40, in agreement with the experimental data. Table 2 reports the relative errors (er) between the length (hr) and the height (h) of the experimental results and the numerical prediction for each of the turbulence models.

#### 4.2 Experiment 6

This experiment consists of the following configuration: initial velocity  $U_i = 2.71$  m/s, depth of supercritical flow  $y_1 = 0.025$  m and Froude number of  $Fr = 5.49$ . The same conclusion made for experiment 3 can be extended to experiment 6, since the RNG  $k-\epsilon$  model gets better alignment with the experimental data, whereas the models  $k-\epsilon$  and SST  $k-\omega$  reproduce similar results to the simulation, as can be seen in Fig. 4. In addition, a slight misalignment is noticed at the beginning of the domain of the three models, including the RNG  $k-\epsilon$  model. The Froude number of this experiment is larger than the previous one, resulting in a higher level of turbulence and hindering the prediction of the variables of interest. Table 3 reports the relative errors for this experiment.

#### 4.3 Experiment 8

This experiment consists had a  $U_i = 3.14$  m/s initial velocity, depth of supercritical flow  $y_1 = 0.015$  m and Froude number of  $Fr = 8.19$ .

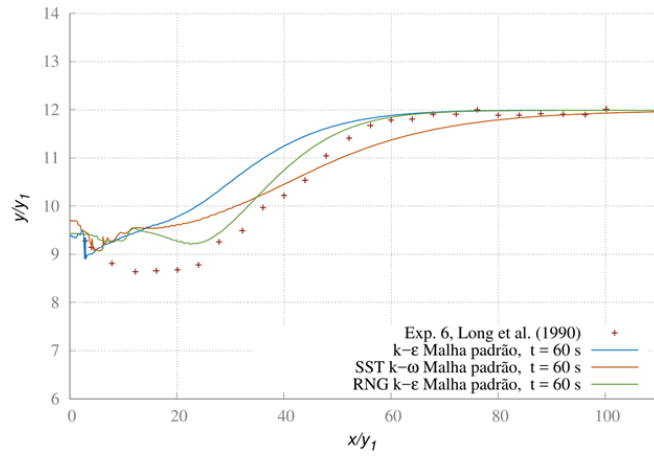


Fig. 4 Turbulence model analysis of experiment 6

Table 3 Relative error - Experiment 6

Model	er (%)	
	Lr	Hr
k- ε	0.26	1.17
SST k-ω	46.58	13.62
RNG k- ε	0.25	1.40

Table 4 Relative error - Experiment 8

Model	er (%)	
	Lr	hr
k- ε	0.13	16.93
SST k-ω	24.68	1.05
RNG k- ε	0.02	10.83

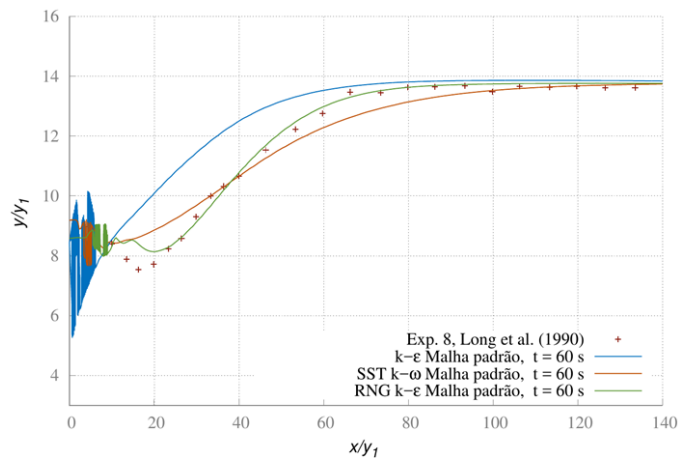


Fig. 5 Turbulence model analysis of experiment 8

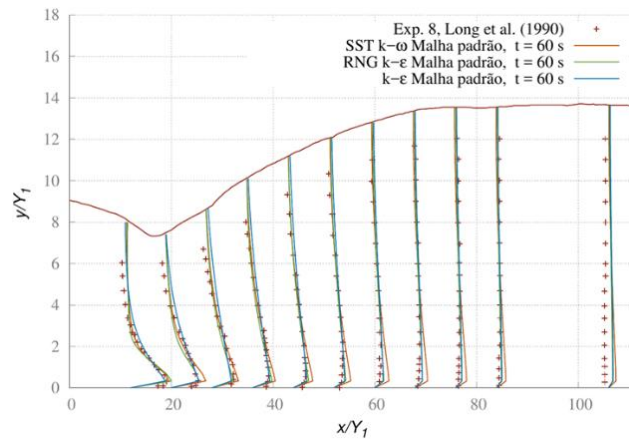


Fig. 6 Longitudinal velocity profiles

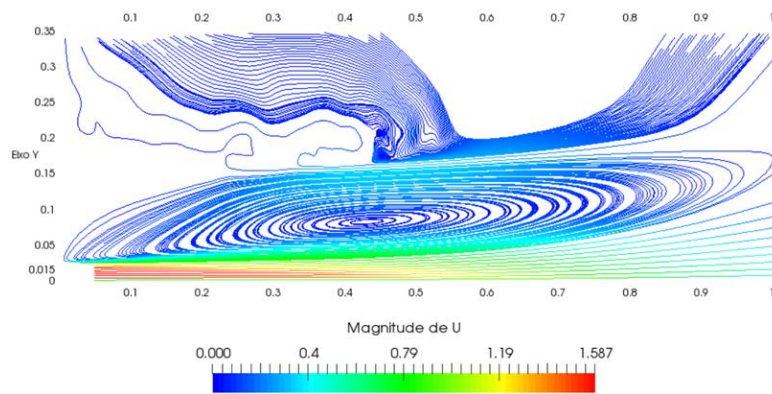


Fig. 7 Stream lines of the submersed hydraulic jump

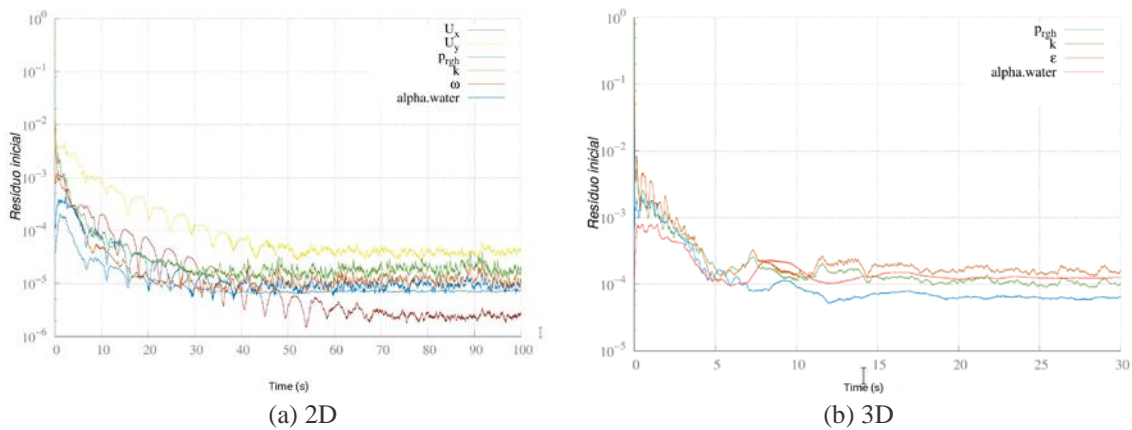


Fig. 8 Residual convergence analysis

It is observed that in Fig. 5, the RNG  $k-\epsilon$  model continues to provide the best fit relative to the experimental data, while the  $k-\epsilon$  and SST  $k-\omega$  display similar results. However, in this

experiment, which consists of a Froude number 8.1, the hydraulic has an even greater chaotic nature. Therefore, there is a greater fluctuation in the capture of the air-water interface at the beginning of the domain because of the bubble dispersion in the highly super-critical flow. However, it was the experiment in which the RNG  $k-\epsilon$  model obtained a better alignment with the experimental data. Table 4 represents the relative errors for this experiment.

In addition, an analysis of the longitudinal velocity ( $U_x$ ) was made for experiment 8 of the three turbulence models, as can be seen in Fig. 6. In this Figure, it can be seen that the longitudinal velocity ( $U_x$ ) of the three models of turbulence does not vary much in relation to the experimental data. The models RNG  $k-\epsilon$  and  $k-\epsilon$  are practically the same, whereas the model SST  $k-\omega$  has a slight deviation. Thus, it can be concluded that any of the three turbulence models are also accurate in relation to the longitudinal velocity of the submerged Froude number 8.19. The hydraulic vorticity are shown in a stream line at the Fig 11. For a initial velocity of  $U_i = 3.14\text{m/s}$ , the supercritical depth flow was  $y_1 = 0.015\text{m}$  and the Froude number  $Fr = 8.19$ . The solution was processed for 60s with a standard mesh refinement for three turbulence models. The numerical convergence of the turbulence SST  $k-\omega$  model is showed in the Fig. 8(a). After 60s the initial residual of the variables are kept constant, under  $e-4$ .

## 5. Tridimensional simulation

Six cases were performed for the analysis of the classical hydraulic jump, coming from the two experiments chosen from Wang *et al.* (2015). Experiments 1 and 3 have Froude 3.1 and 7.1, respectively. For each, a comparative analysis of the turbulence models was performed. For the three-dimensional numerical simulation the data were compared with [12]. Four experiments of the classic hydraulic jump were performed. Two simulations of Froude number 3.1 and 7.5 were planned for the comparison of the turbulence models. The numbering of the experiments were maintained as cited in (Wang *et al.* 2015).

### 5.1 Experiment 1

This experiment had a  $U_i = 1.74\text{ m/s}$  initial velocity, depth of supercritical flow  $y_1 = 0.02\text{ m}$  and Froude number of  $Fr = 3.1$ . The solution was run to 30 s with the standard mesh refinement for the three turbulence models.

None of the three Turbulence models have a good alignment with the experimental data. In addition, the turbulence model RNG  $k-\epsilon$ , which previously obtained good results with the two dimensional data, is as less accurate as the SST  $k-\omega$  model and the turbulence model that best suits the three-dimensional case of experiment 1, is the model  $k-\epsilon$ . A Table 6 reports the relative errors ( $er$ ) for this experiment, confirming analytically, that the  $k-\epsilon$  model stands out among the others.

Table 5 Three-dimensional simulation setup. Adapted from (Wang *et al.* 2015)

Experiment	$y_1$ (m)	$d_1$ (m/s)	$y_2$ (m)	$U_1$ (m/s)	$F_1$	$Re(\times 10^{-3})$
1	0.02	0.0206	0.1040	1.74	3.1	$3.5 \times 10^4$
3	0.02	0.0206	0.2053	3.37	3.37	$6.8 \times 10^4$

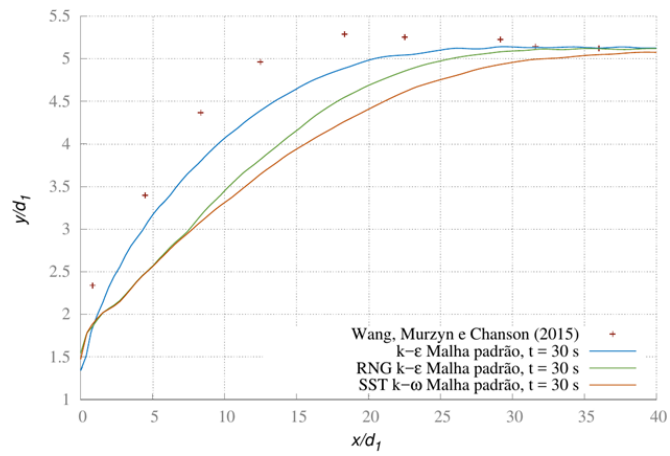


Fig. 9 Turbulence model comparison

Table 6 Relative error - Experiment 8

Model	er (%)	
	Lr	hr
k- $\epsilon$	1.13	3.42
SST k- $\omega$	40.73	2.17
RNG k- $\epsilon$	26.87	0.31

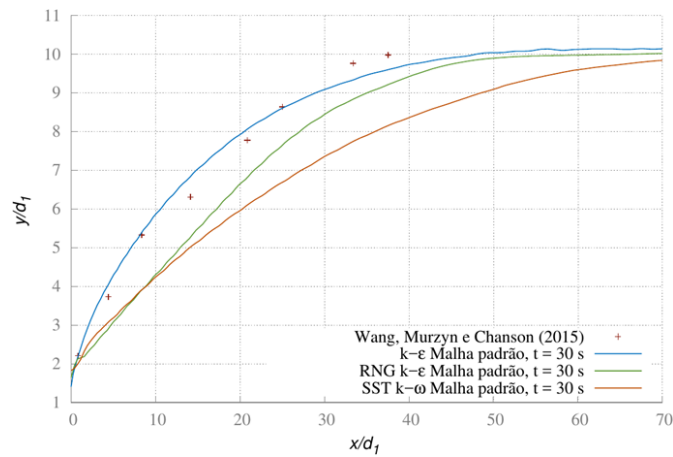


Fig. 10 Turbulence model comparison-Experiment 3-Tridimensional case

Table 7 Relative Error - experiment 3 - Tridimensional case

Model	er (%)	
	Lr	hr
k- $\epsilon$	26.57	7.51
SST k- $\omega$	85.32	4.50
RNG k- $\epsilon$	34.97	5.88

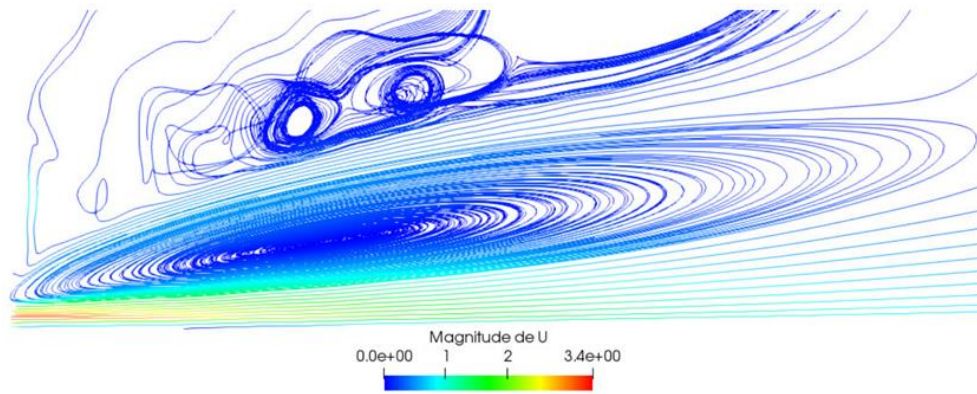


Fig. 11 Flow stream lines - Tridimensional case

### 5.2 Experiment 3

The experiment consists of a  $U_i = 3.37$  m/s initial velocity,  $y_1 = 0.02$  m depth of supercritical flow and  $F_r = 7.5$  Froude number. For this experiment, the turbulence model  $k-\epsilon$  obtained good results in relation to the experimental data, as can be seen in Fig. 10. The Table 7 reports that the  $L_r$  and  $h_r$  variables have worse results. It is possible to check the vorticity lines at this case at Figure 11. Similar to the two-dimensional case, a qualitative analysis was performed to verify the behavior of a hydraulic jump phenomenon. The Froude number adopted for the results showed below was 7.5.

Similar to the two-dimensional case, the same procedure to guarantee the numerical convergence was made for the three-dimensional case as showed in Fig. 8(b). It is observed that from 15s the solution is stable with the residues below  $e^{-3}$ .

## 6. Conclusions

Choosing the best turbulence model for CFD codes among a large number of options is crucial, however, it can be a tricky activity due mainly to strong dependence on particular cases. In the literature, it is found that the RNG  $k-\epsilon$  turbulence model is most commonly used for hydraulic application. In spite of this, this work carried out fifteen simulations to compare which of the three models of turbulence mentioned has a better prediction in the hydraulics. For the two dimensional modeling, the turbulence model RNG  $k-\epsilon$  showed to be the most suitable model to the air-water interface height ( $h_r$ ) and length of the jump ( $L_r$ ) prediction. For the three-dimensional modeling, the turbulence model  $k-\epsilon$  seems to be more appropriate in respect of the length of the hydraulic jump ( $L_r$ ) adjustment.

## Acknowledgments

Some of this work benefited from the support of Rio de Janeiro Federal University computer resources at Thermal and Fluid Mechanics Laboratory. The research is part of the Advanced Computational Fluid Dynamics project financed by Foundation for Research Support of Rio de

Janeiro State – FAPERJ.

## References

- Abrunhosa, J.D.M. (2003), “Simulação de escoamento turbulento complexo com modelagem clássica e de grandes escala”, Ph.D. Dissertação, Pontifícia Universidade Católica do Rio de Janeiro, Rio de Janeiro, Brazil.
- Baek, H. and Karniadakis, G.E. (2012), “A convergence study of a new partitioned fluid-structure interaction algorithm based on fictitious mass and damping”, *J. Comput. Phys.*, **231**(2), 629-652. <https://doi.org/10.1016/j.jcp.2011.09.025>.
- Bayon, A. and Lopez, P.A. (2015), “Numerical analysis of hydraulic jumps using OpenFOAM”, *J. Hydroinform.*, **17**(4), 662-678. <https://doi.org/10.2166/hydro.2015.041>.
- Chow, V.T. (1959), *Open-Channel Hydraulics*, McGraw-Hill, New York, U.S.A.
- Hirt, C.W. and Nichols, B.D. (1981), “Volume of fluid method for the dynamics of free boundaries”, *J. Comput. Phys.*, **39**(1), 201-225. [https://doi.org/10.1016/0021-9991\(81\)90145-5](https://doi.org/10.1016/0021-9991(81)90145-5).
- Long, D., Steffler, P.M. and Rajaratnam, N. (1990), “LDA study of flow structure in submerged hydraulic jump”, *J. Hydraul. Res.*, **28**(4), 437-460. <https://doi.org/10.1080/00221689009499059>.
- McCarthy, M.F. and O’Leary, P.M. (1978), “The growth and decay of a hydraulic jump”, *J. Hydrol.*, **39**(3), 273-285. [https://doi.org/10.1016/0022-1694\(78\)90005-7](https://doi.org/10.1016/0022-1694(78)90005-7).
- Piomelli, U. (1999), “Large-eddy simulation: Achievements and challenges. Progress in Aerospace Sciences”, *Int. J. Numer. Anal. Meth. Eng.*, **35**(4), 335-362. [https://doi.org/10.1016/S0376-0421\(98\)00014-1](https://doi.org/10.1016/S0376-0421(98)00014-1).
- Versteeg, H.K. and Malalasekera, W. (1995), *An Introduction to Computational Fluid Dynamics: The Finite Volume Method*, Addison-Wesley-Longman, 1-257.
- Wang, H., Murzyn, F. and Chanson, H. (2015), “Interaction between free-surface, two-phase flow and total pressure in hydraulic jump”, *Exper. Therm. Fluid Sci.*, **64**, 30-41. <https://doi.org/10.1016/j.expthermflusci.2015.02.003>.
- Wang, W., Zhang, L.X., Yan, Y. and Guo, Y. (2012), “Combined multi-predict-correct iterative method for interaction between pulsatile flow and large deformation structure”, *Coupled Syst. Mech.*, **1**(4), 361-379. <https://doi.org/10.12989/csm.2012.1.4.361>.
- Yakhot, V. and Smith, L.M. (1992), “The renormalization group, the  $\epsilon$ -expansion and derivation of turbulence models”, *J. Sci. Comput.*, **7**(1), 35-61. <https://doi.org/10.1007/BF01060210>.

AI